DE GRUYTER
OPEN

Contributions to Geophysics and Geodesy Vol. 45/2, 2015 (149–171)

Deformation induced topographic effects in inversion of temporal gravity changes: First look at Free Air and Bouguer terms

Peter VAJDA[1,*], Pavol ZAHOREC Pavol[1], Juraj PAPČO[2], Anna KUBOVÁ[1]

[1] Earth Science Institute, Slovak Academy of Sciences,
Dúbravská cesta 9, P.O. Box 106, 840 05 Bratislava, Slovakia

[2] Department of Theoretical Geodesy, Faculty of Civil Engineering,
Slovak University of Technology, Radlinského 11, 813 68, Bratislava, Slovak Republic

[*]Corresponding author, Email: Peter.Vajda@savba.sk, Fax: +421 2 59410 607

Abstract: We review here the gravitational effects on the temporal (time-lapse) gravity changes induced by the surface deformation (vertical displacements). We focus on two terms, one induced by the displacement of the benchmark (gravity station) in the ambient gravity field, and the other imposed by the attraction of the masses within the topographic deformation rind. The first term, coined often the Free Air Effect (FAE), is the product of the vertical gradient of gravity (VGG) and the vertical displacement of the benchmark. We examine the use of the vertical gradient of normal gravity, typically called the theoretical or normal Free Air Gradient (normal FAG), as a replacement for the true VGG in the FAE, as well as the contribution of the topography to the VGG. We compute a topographic correction to the normal FAG, to offer a better approximation of the VGG, and evaluate its size and shape (spatial behavior) for a volcanic study area selected as the Central Volcanic Complex (CVC) on Tenerife, where this correction reaches 77% of the normal FAG and varies rapidly with terrain. The second term, imposed by the attraction of the vertically displaced topo-masses, referred to here as the Topographic Deformation Effect (TDE) must be computed by numerical evaluation of the Newton volumetric integral. As the effect wanes off quickly with distance, a high resolution DEM is required for its evaluation. In practice this effect is often approximated by the planar or spherical Bouguer deformation effect (BDE). By a synthetic simulation at the CVC of Tenerife we show the difference between the rigorously evaluated TDE and its approximation by the planar BDE. The complete effect, coined here the Deformation Induced Topographic Effect (DITE) is the sum of FAE and TDE. Next we compare by means of synthetic simulations the DITE with two approximations of DITE typically used in practice: one amounting only to the first term in which the VGG is approximated by normal FAG, the other adopting a Bouguer corrected normal FAG (BCFAG).

Key words: microgravimetry, temporal gravity change, vertical displacement, vertical gradient of gravity, topographic effect, interpretation

doi: 10.1515/congeo-2015-0018

1. Introduction

Volcanic unrest and activity are typically accompanied by temporal gravity changes Δg and ground deformations (inflation/deflation) causing vertical displacements, i.e., elevation changes Δh of the topographic surface. The ground deformation produces gravity effects that contribute to the observed gravity changes. When gravity changes are inverted and interpreted as a stand-alone quantity, seeking the subsurface mass-density changes in volcanic areas, the deformation-induced gravity effects must be removed from the observed gravity changes beforehand as corrections (reductions) in the data processing step. Based on synthetic case studies, using the Mogi source of pressure/dilation, along with high resolution digital terrain models, we assess these deformation-induced topographic effects numerically. Our objective is to evaluate their magnitude and spatial behavior, as well as to compare them with their typical approximations.

2. Decomposition of gravity changes – corrections (reductions) and sought signal

The temporal gravity changes are a composite signal, due to superposition of various subsurface, surface and environmental effects. In general they may be caused by the following effects (e.g., *Battaglia et al., 2008, Eq. (1) and Fig. 1; Jousset et al., 2000, Eq. (1) and Fig. 1;* cf. also *Berrino et al., 1984, 1992; Eggers, 1994; Rymer 1994; Jousset and Okada, 1999; Currenti et al., 2007, 2008; Trasatti and Bonafede, 2008; Battaglia and Hill, 2009*):

a) Tidal and atmospheric effects (Δg^{ext})
b) Instrument/survey effects (Δg^{inst})
c) Hydrological effects (Δg^{w})
d) Deformation-induced topographic effects (Δg^{def})
e) Subsurface (underground) effects related to volcanic processes (Δg^{res})
f) Surface effects related to volcanic processes (Δg^{surf}).

By tidal effects we mean solid earth (body) tides, and ocean loading effects. By atmospheric effects we mean gravity changes induced by pressure and

temperature changes in the atmosphere (atmospheric attraction and loading effects). These effects are known and respective corrections have been published (e.g., *Wahr, 1981; Dehant, 1987; Merriam, 1992; Wenzel 1996; Boy et al., 2002; Riccardi et al., 2008*).

Under instrument/survey effects are usually listed the drift of gravimeters and adjustment of redundant measurements. We want to highlight one particular effect that must not be neglected in monitoring and interpreting time-lapse gravity change observations. Various gravimeters have various heights of the sensor, measured from the bottom of the instrument. In addition, various plates or tripods can be used, implying various height of the bottom of the instrument above a benchmark (gravity station, gravity point). If various types of gravimeters or plates/tripods are used within an epoch survey or between epochs, observed gravity must be reduced to the elevation of the benchmark. Otherwise significant systematic errors could be introduced. In order to reduce the meter reading to the ground, actual vertical gradient of gravity (VGG) is needed. It may be either observed at each station, or estimated, as will be discussed further below (cf. also *Zahorec et al., 2014*).

Under hydrological effects we mean the changes in the groundwater table level as well as in the soil/rock moisture (due to precipitation/drought). Strictly speaking to correct for this environmental signal, detailed 3D modelling needs to be performed, which is typically unachievable due to lack of required input data and/or knowledge about the subsurface structure. Various approximations and estimates are used in practice; data on water table from wells are used wherever available. The simplest approximation is a planar Bouguer effect of a water table level change (e.g., *Battaglia et al., 2003, Appendix*). This hydrological correction is not the subject of our interest here, we refer the reader to published work (e.g., *Krause et al., 2009; Leirião et al., 2009; Lampitelli and Francis, 2010*).

Deformation-induced topographic effects are the core focus of our work. They are treated in the next section.

Under subsurface effects related to volcanic process we mean mass changes due to magma migration (rejuvenation or drainage of existing reservoirs and paths, intrusion/propagation along new paths, such as diking, etc.), hydrothermal fluids (volatiles) migration, density changes due to physical and chemical (compositional) changes of present magma (cooling, heating, vesic-

ulation, degassing, fractional crystallization, differentiation, mixing, etc.), density changes of the geological structure of the edifice due to stress induced strain field (including the deformation of density interfaces) and due to temperature field changes via thermal expansivity. All of these changes represent the net sought signal, which in its nature is a fairly complex composite signal itself. This component of the gravity changes, typically called "residual gravity changes" is the subject of inversion or forward modeling and of subsequent interpretation of magma-related processes.

Under the surface effects we mean gravitational effects of mass changes taking place on the surface, but not related to surface deformation, such as magma extrusion, dome growth, dome collapse, lava flow, lahar, flank collapse, etc. These masses can be surveyed on the surface, their shapes and sizes digitized, their gravitational effects computed by a numerical realization of the Newton volume integral for the vertical component of the attraction, and subsequently subtracted (corrected for). This may be achieved with the help of photogrammetry, laser scanning, LIDAR, etc. These corrections are out of scope of our interest in this paper. We refer the reader to published work (e.g., *Jousset et al., 2000; Schiavonne et al., 2009*).

The net signal to be inverted/interpreted is thus represented by the residual gravity changes (Δg^{res}) obtained after applying all the necessary corrections/reductions to the observed gravity changes (Δg^{obs}):

$$\Delta g^{res} = \Delta g^{obs} - \Delta g^{ext} - \Delta g^{inst} - \Delta g^{w} - \Delta g^{def} - \Delta g^{surf} \,. \tag{1}$$

3. Deformation-induced topographic effects on time-lapse gravity change

In this section we shall pay attention to the component of gravity changes imposed by the vertical displacement of the topographic surface (such as inflation). During the deformation, the gravity station (benchmark) is vertically displaced together with the topographic surface. We note that the subsurface density (geological) structure is deformed, too, but this effect we treat as part of the net signal (Δg^{res}). We can hypothetically split the ground deformation effect into two subsequent processes (steps) with their respective effect components: In the first step we move the benchmark vertically from its original position (P) on the pre-deformation topographic

surface (say prior to inflation) to its new post-deformation position (P^*) in the ambient gravity field (in "free air") without deforming (inflating) the topographic surface, yet. In the second step we move (deform, inflate) the topographic masses. Thus we can write for these two separated components:

$$\Delta g^{def}(P^*) = \Delta g^{FAE}(P^*) + \Delta g^{TDE}(P^*)\,, \tag{2}$$

where Δg^{def} is the Deformation Induced Topographic Effect (DITE), Δg^{FAE} is the gravity change due to the vertical displacement of the benchmark in ambient gravity field (in "free air"), in the sequel referred to as the "Free Air Effect" (FAE), and Δg^{TDE} is the gravitational effect (vertical component of the attraction vector) of the topographic masses that were displaced into the volumetric domain between the pre- and post-deformation topographic surfaces In the sequel we shall refer to it as the "Topographic Deformation Effect" (TDE) Under certain assumptions it may be approximated by an effect referred to as the "Bouguer Deformation Effect" (e.g., *Battaglia et al., 2008*) This approximation, referred to as "BDE", will be examined below.

3.1 Free Air Effect and its approximations

The first term on the right-hand side of Eq. (2), constitutes the effect of displacing the benchmark in the ambient gravity field. It amounts to the vertical displacement of the benchmark (Δh) times the true VGG ($\partial g/\partial h$):

$$\Delta g^{FAE}(P^*) = (\partial g/\partial h)^o\,(P) * \Delta h(P)\,. \tag{3}$$

Inevitably, the VGG must be observed in situ at the benchmark (hence the superscript "o"). This can be practically achieved by relative gravimeters observing in a so called tower mode, i.e., on the ground and at a certain height above the benchmark, such as 1 m, on a tripod (e.g., *Zahorec et al., 2014*). For instance considering the accuracy of a gravimeter at the level of 5 μGal in each position, the accuracy of the measured VGG is estimated at the level of 7 μGal/m. Besides the measurement error, we are aware that the VGG is also a function of the height above the ground, so our measurement is only the approximation of its true value.

If the VGG is not observed in situ, it is often approximated by the "theoretical free air gradient" (theoretical FAG), also called the "normal FAG"

(e.g., *Berrino et al., 1992; Rymer, 1994*), which is the gradient of normal gravity at the surface of the normal reference ellipsoid. In the sequel we shall abbreviate the normal FAG as NFAG (NFAG $= -308.6$ μGal/m). The approximation of the VGG by NFAG results in the following approximation of the FAE:

$$\Delta g^{FAE}(P^*) \approx \Delta g^{NFAE}(P^*), \quad \Delta g^{NFAE}(P^*) = NFAG * \Delta h(P)\,. \tag{4}$$

Observations indicate that the approximation of the true VGG by the NFAG can introduce a relative error of up to 88 % of the FAE in rugged terrain (*Zahorec et al., 2014*). They report values of the VGG for the alpine mountainous regions of Slovakia that vary from -580 to -132 μGal/m.

Therefore we propose a better approximation of the true VGG, in case it is not observed, than the NFAG. In rugged terrain regions the strongest (primary) contribution to the VGG comes from the terrain (topography, and eventually also bathymetry for near shore benchmarks) from within the very near vicinity of the benchmark. This contribution can be modelled (adopting a constant topo-density) using precise high resolution digital terrain models (*ibid*). The NFAG can be refined (corrected for) using this ***topographic contribution to the VGG*** (ΔFAG^T), yielding a refined approximation of the FAE:

$$\begin{aligned} &\Delta g^{FAE}(P^*) \approx \Delta g^{TNFAE}(P^*)\,, \\ &\Delta g^{TNFAE}(P^*) = (NFAG + \Delta FAG^T(P)) * \Delta h(P)\,. \end{aligned} \tag{5}$$

In the sequel we shall abbreviate the "topo-corrected NFAG" as "TNFAG". In section 4.1 we show numerical values of the TNFAG for the Central Volcanic Complex (CVC) of Tenerife, Canary islands. The secondary contribution to the true VGG comes from the underground geological structure (density anomalies) of the earth (ΔFAG^G), as $VGG = NFAG + \Delta FAG^T + \Delta FAG^G$. This contribution typically remains unmodelled, as the structure is unknown. Alternatively, *Berrino et al. (1992)* and *Rymer (1994)* propose an approximation (of the VGG), a refinement to FAG, based on the Bouguer anomaly map of the area. The contribution of geology to FAG in volcanic areas with significant (rugged) topography is expected to be smaller than that of topography, although in flat areas (such as calderas) the situation may be vice versa.

3.2. Topographic Deformation Effect and its Bouguer approximation

The gravitational effect (attraction) of the masses between the topographic surfaces prior to and after the deformation (within the topographic deformation shell), on the observed gravity change at each benchmark of the survey, can be computed by numerical evaluation of the Newton integral (for vertical component of the attraction vector) over this volumetric domain with assumed mean constant topographic density (of volcanic edifice rock environment). In section 4.2 we illustrate this effect at the CVC of Tenerife, for a synthetic deformation (surface displacement) field generated by two (shallow and deep) Mogi sources.

This Topographic Deformation Effect (TDE), is typically approximated by a Bouguer plate effect (e.g., *Berrino et al., 1992; Rymer, 1994*), hence the name "Bouguer deformation effect" (BDE),

$$\Delta g^{TDE}(P^*) \approx 2\pi G\rho_0 * \Delta h(P)\,, \tag{6}$$

implying the "Bouguer gradient" $BUG = 2\pi G\rho_0$, where G is the gravitational constant ($6.67 \times 10^{-11}\mathrm{Nm}^2/\mathrm{kg}^2$) and ρ_0 is the average constant onsite density of the topographic masses (edifice rock). Alternatively, the TDE is approximated by a "point source effect" (of uplift due to dilatation/pressure), the Mogi point source effect (e.g., *Rymer, 1994; Williams-Jones and Rymer, 2002*):

$$\Delta g^{TDE}(P^*) \approx (4/3)\pi G\rho_0 * \Delta h(P)\,, \tag{7}$$

implying a different Bouguer gradient, $BUG = (4/3)\pi G\rho_0$ usually referred to as the "spherical BUG". However, the effect given by Eq. (7), is actually a superposition (sum) of three effects (*Jousset and Okada, 1999*, Eqs. (1) and (2)): the Bouguer plate effect, the volume change effect, and the density change effect (cf. *Hagiwara, 1977*), all due to the Mogi source. For this reason, and in order to distinguish it from the Bouguer plate deformation effect, it should be better referred to as the "Mogi-Bouguer deformation effect" implying a "Mogi-Bouguer gradient (MBUG)". Notice that both BUG and MBUG (as constants) are (constant average topo-) density dependent.

In section 4.2 we show also the difference between the TDE computed by numerical integration of the Newton volumetric integral and its Bouguer

plate approximation (BDE), for a synthetic displacement field within the CVC of Tenerife, produced by the two above mentioned Mogi sources.

Since both approximations of the TDE, given by Eqs. (6) and (7), depend linearly on the benchmark-specific surface displacement $\Delta h(P)$, and so does the FAE in which the VGG is approximated by NFAG, the Free Air and Bouguer Deformation effects can then (when approximated) be merged into one effect, and consequently one can work with "Bouguer corrected" (modified, refined) Free Air Gradients "BCFAG" (e.g., *Berrino et al., 1992; Rymer, 1994; Williams-Jones and Rymer, 2002; Gottsmann et al., 2003*) that are constant (only density (ρ_0) dependent):

$$\left(\frac{\Delta g^{def}}{\Delta h}\right)(P) = BCFAG(\rho_0)\,, \tag{8}$$

where $BCFAG = NFAG + BUG$ or $BCFAG = NFAG + MBUG$ (cf. Eq. (6) or (7)). Consequently, "residual gravity gradients" can be constructed and used in the joint interpretation of observed gravity changes and surface displacements (deformations), e.g. (*ibid*):

$$\left(\frac{\Delta g^{res}}{\Delta h}\right)(P) = \left(\frac{\Delta g^{obs}}{\Delta h}\right)(P) - BCFAG(\rho_0)\,. \tag{9}$$

In addition, the theoretical FAG (NFAG) within the BCFAG, is in some studies replaced by some average (constant) FAG estimated or calculated for the volcanic site under study such as an entire caldera (*ibid*). The quoted authors propose the above approximations in volcanic areas of relatively flat topography, such as some calderas. They also stress that observed in situ VGGs should be used in more pronounced topographies.

4. Synthetic case study: Central Volcanic Complex of Tenerife

We have chosen for our synthetic simulations the central volcanic complex (CVC) on Tenerife, Canary Islands, Spain (Fig. 1), as it comprises a caldera (Las Cañadas) at the altitude of roughly 2000 m a.s.l., and twin stratovolcanoes, Teide and Pico Viejo, within it. This study area contains high altitudes, rugged terrain, and has features characteristic of many volcanic areas. During the volcanic unrest of 2004–2005, spatio-temporal gravity

changes were observed (*Gottsmann et al., 2006*), at 14 benchmarks of the rapid reaction CVC network, accompanied by no statistically significant areal surface deformations (within the average precision of the elevation control of ±3 cm). Since the area did not experience widespread ground deformation, there was no need to correct for the deformation-induced topographic effects when inverting and interpreting the gravity changes of the unrest (*Gottsmann et al., 2006; Prutkin et al., 2014*). Only a few benchmarks experienced local vertical displacements denoted by *Gottsmann et al. (2006)* as site effects. Those were reduced using the normal (theoretical) FAG.

For our synthetic simulations we use a DEM (Fig. 2) derived from LIDAR measurements. Original data were obtained from the Spanish National Geographic Institute and the National Geographic Information Centre (Instituto Geografico Nacional, Centro Nacional De Informacion Geografica (CNIG) http://www.ign.es/). The Lidar data were acquired in 2009 within the National Plan of Air Orthophotography (Plan Nacional de Ortofotografía Aérea PNOA) project (http://pnoa.ign.es/) with a density of 0.5 points/m and vertical accuracy better than 20 cm RMS. Point clouds have been captured by LiDAR sensors and then automatically classified and colored in RGB derived from the PNOA orthophotos with pixel size of 25 or 50 cm. Data were distributed in LAZ format through the center CNIG in 2×2 km tiles. The geodetic reference system is the REGCAN95 with UTM

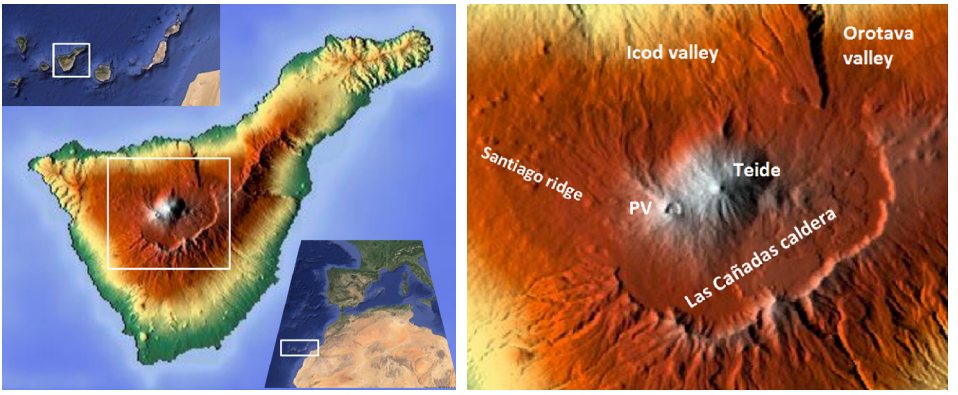

Fig. 1. (a) Location of the Canary islands and Tenerife, (b) the CVC of the caldera and the twin stratovolcanoes Teide and Pico Viejo (PV).

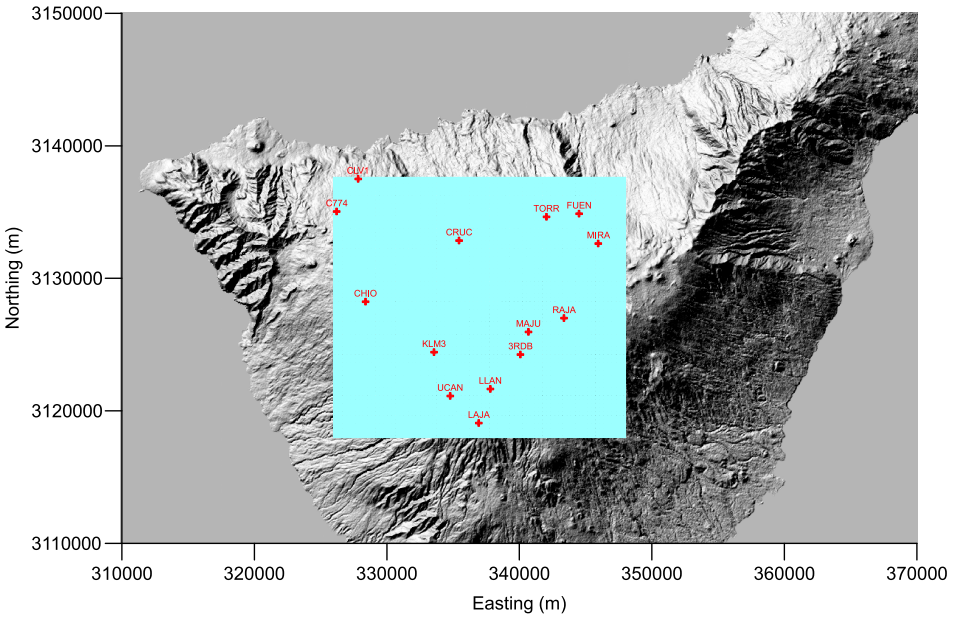

Fig. 2. The DEM of Tenerife and our study area (blue rectangle) for our synthetic simulations (grid step of 100 m). The positions of the 14 benchmarks of the gravimetric network of the CVC are marked by red crosses.

projection. Orthometric heights are transformed from ellipsoidal using the EGM2008-REDNAP geoid. Manipulation with data and production of the final grid were performed in Surfer using the Kriging interpolation procedure. The blue rectangle in Fig. 2 shows our study area, while the network of benchmarks is shown in red.

4.1 Free Air Effect

The FAE has to be computed using the true (observed) VGG, cf. Eq. (3). In cases where the observed VGG is not available, we propose to approximate it by TNFAG, i.e., by NFAG refined with the topographic contribution (ΔFAG^T). The contribution of the near topography and bathymetry to the NFAG was computed by a simple approach as a difference between topographic (and bathymetric) effects calculated at two vertically separated points, namely at points lying at 1.25 m and 0.25 m above the topographic

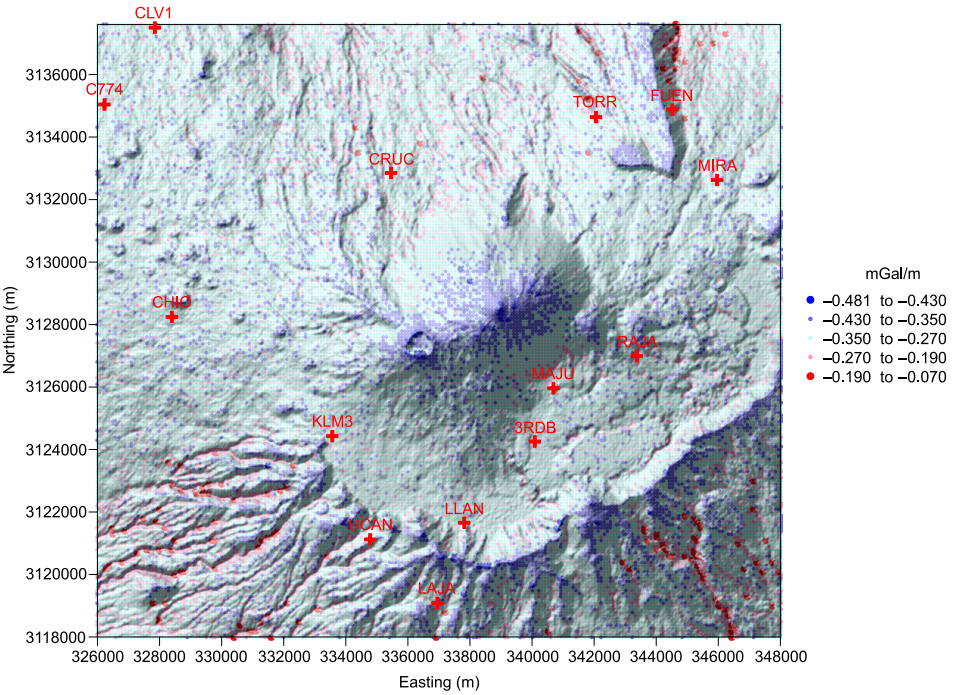

Fig. 3. Topo-corrected normal FAG (TNFAG) values. Minima (in absolute value) correspond with sharp concave topo-features (valleys, gullies, drains), while maxima (in absolute sense) with sharp convex topo-features (peaks, ridges, pillars, crests, ribs). Max = −70, Min = −481, Mean = −315, SD = 34 (μGal/m).

surface, respectively (the 25 cm being a standard height of the gravity sensor in case of Scintrex CG-5/3 gravity meters). We calculate the topographic/bathymetric effect standardly up to the distance of 166.7 km using the software Toposk (*Marušiak et al., 2013*). The calculation area is divided into four circular subzones: T1 (0–250 m), T2 (250–5240 m), T31 (5.24–28.8 km) and T32 (28.8–166.7 km). Within the zones T1 and T2 it is necessary to use a very detailed digital elevation model (DEM). We have used the DEM derived from LIDAR data available from the Spanish National Geographic Institute, described above. The contributions of topographic and bathymetric effects from outer zones T31 and T32 were calculated using the SRTM data (*Jarvis et al., 2008* and *Becker et al., 2009*) with resolutions 3 and 15 seconds, respectively. The outer zones contribute to the ΔFAG^T

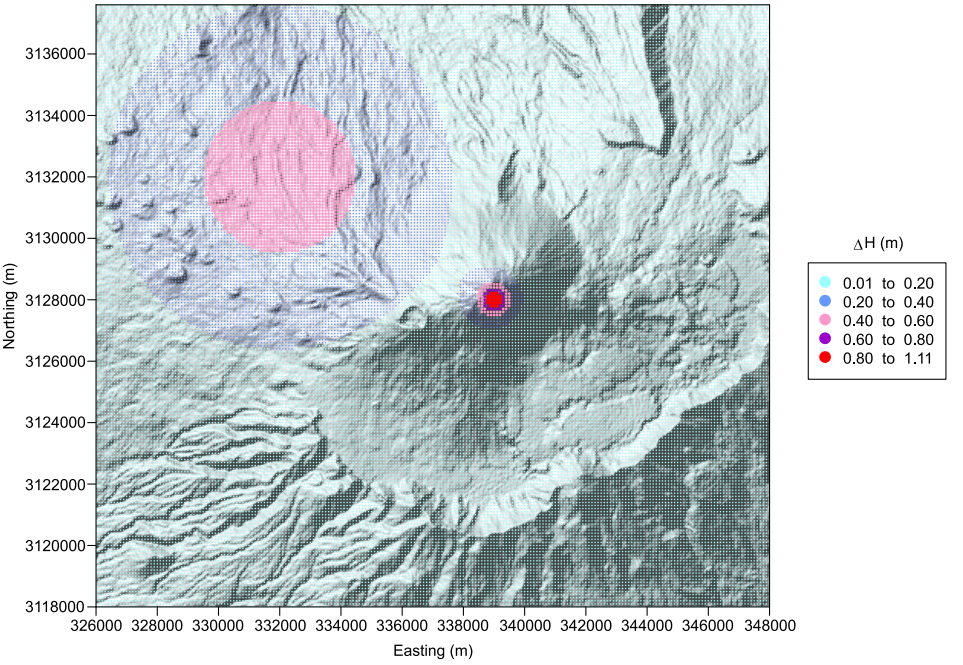

Fig. 4. Synthetic vertical surface displacements at the CVC of Tenerife produced by two Mogi sources: a shallow source located at the depth of 500 m roughly below the Teide summit scaled to have a displacement magnitude of 1 m, and a deep source, located at the depth of 6 km roughly 5 km to the NW of the twin stratovolcanoes, scaled to have a displacement magnitude of 50 cm.

values usually only by several percent (several μGal/m). We have used the density of topographic masses equal to 2200 kg/m^3 reported by *Gottsmann et al. (2008)*. The topo-corrected NFAG (Fig. 3) values vary from -481 to -70 μGal/m, which represents a variation of up to 77 % of the normal FAG.

4.2 Topographic Deformation Effect

To compute the TDE via numerical evaluation of the Newton integral for the vertical component of attraction over the volumetric domain enclosed between the pre- and post-deformation topographic surfaces, with a pre-selected 2200 kg/m^3 constant average regional density of the topographic masses (*Gottsmann et al., 2008*), we simulate ground inflation (surface ver-

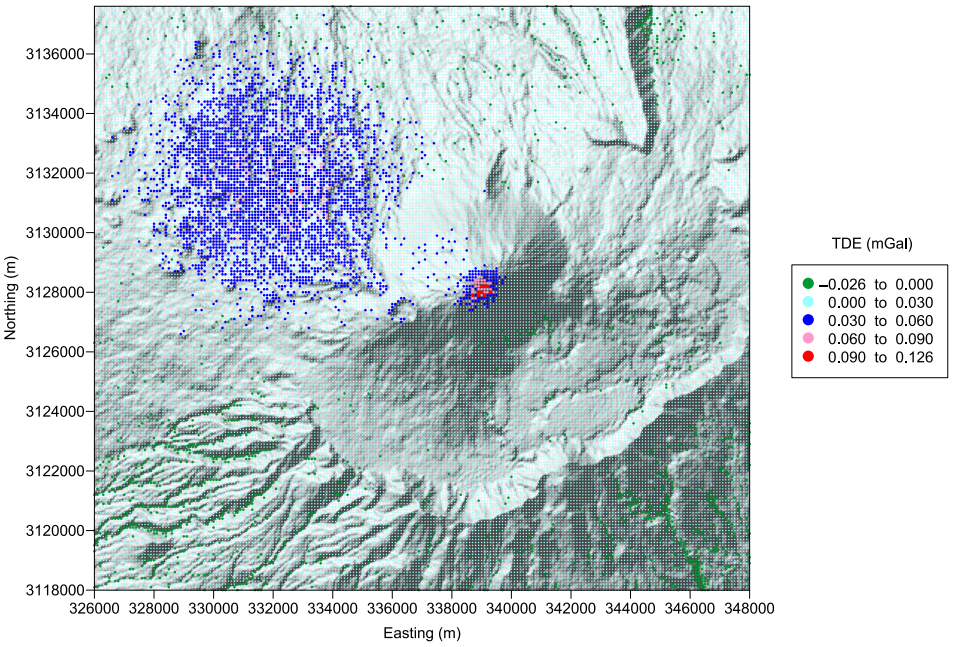

Fig. 5. The Topographic Deformation Effect (TDE) respective to the vertical surface displacement field of Fig. 4, calculated for density 2200 kg/m^3. Max = 126, Min = −26, Mean = 10, SD = 11 (μGal).

tical displacement field) using Mogi point sources (*Mogi, 1958*) of dilatation (of pressure). To have a variety, we use a combination of a shallow source at 500 m depth roughly below the summit of the Teide volcano (UTM easting 339 km, northing 3128 km) with a maximum amplitude of displacement set to 1 m, and a deep source located within the Santiago rift zone (UTM easting 332 km, northing 3132 km) at the depth of 6 km with a displacement magnitude of 50 cm. We neglect topographic heights in the computation of the displacements: they are computed as if on the surface of a halfspace, and then superimposed over the topography. The displacement field, respective to the two described Mogi sources, is presented in Fig. 4. The TDE computed for this displacement field is given in Fig. 5. We also show in Fig. 7 the difference between the TDE computed by Newton volumetric integration (Fig. 5) and its approximation by planar Bouguer deformation effect (Eq. (6)), the BDE shown in Fig. 6.

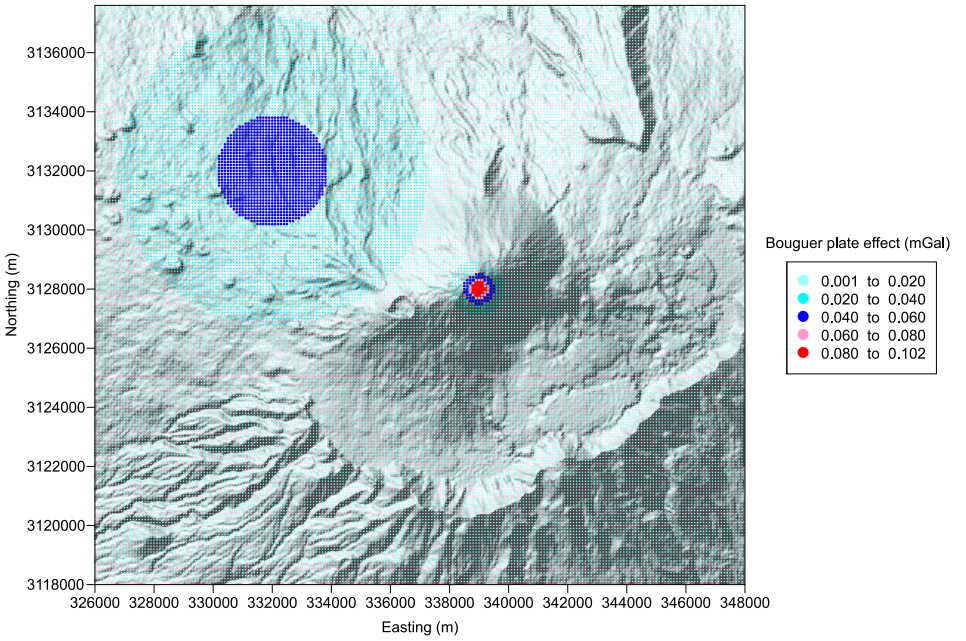

Fig. 6.The approximation of the TDE by the planar Bouguer deformation effect (BDE), respective to the vertical surface displacement field of Fig. 4. Max = 102, Min = 1, Mean = 12, SD = 11 (μGal).

4.3 Deformation-induced topographic effect (DITE) on gravity change

The deformation induced topographic effect (DITE) on gravity change, given by Eq. (2), is the sum of the FAE (section 4.1) and the TDE (section 4.2). Since we do not have the true (observed) VGG values for our study area available, we approximate the VGG values by the topo-corrected normal FAG (TNFAG) values (cf. Fig. 3) in the FAE term when computing the DITE. Thus when we speak in the sequel about the computed DITE, we actually, strictly speaking, mean the "TN-DITE", i.e. that in which the FAE term is predicted using NFAG and the topographic contribution to the VGG. To illustrate the spatial behavior and size of TN-DITE, we compute it for the synthetic displacement field of Fig. 4 generated by the two Mogi sources, see Fig. 8.

Next we want to compare the DITE (herein represented by the TN-

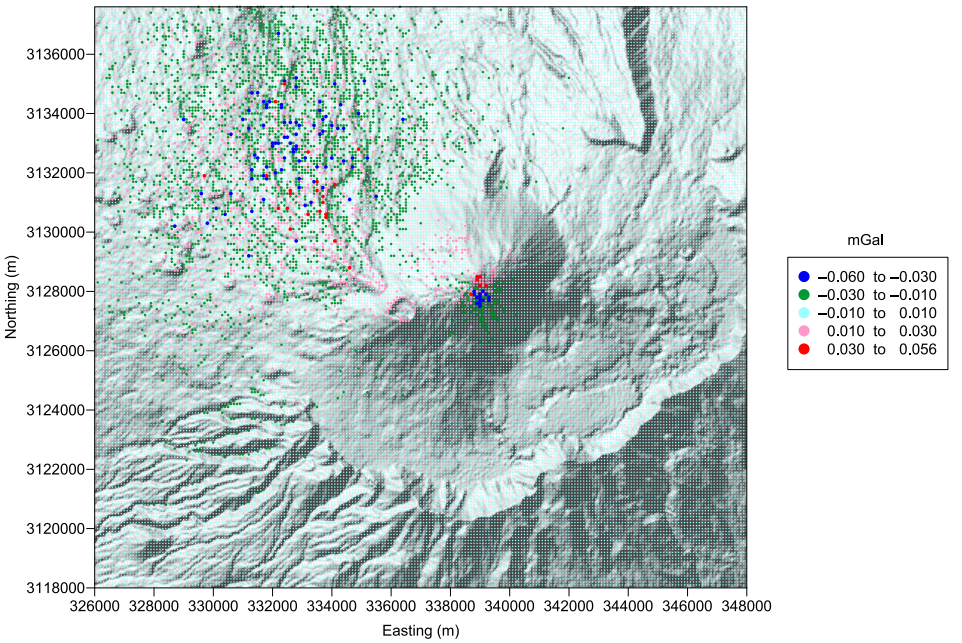

Fig. 7. The difference between the TDE (Fig. 5) and its approximation by the BDE (Fig. 6), both respective to the displacement field of Fig, 4. Max = 56, Min = −60, Mean = −1, SD = 6 (μGal).

DITE) with two of its approximations commonly used in practice, namely the NFAG and BCFAG approximations of DITE. In Fig. 9 we show the DITE approximated by only the first (FAE) term in which moreover NFAG replaces (approximates) the VGG:

$$\Delta g^{def}(P^*) \approx NFAG * \Delta h(P)\,, \tag{10}$$

computed for the displacement field of Fig. 4. The difference between the DITE (herein represented by the TN-DITE of Fig. 8) and the NFAG approximation of DITE (Fig. 9) is shown in Fig. 10.

In Fig. 11 we show the DITE approximated as follows: The VGG in the FAE term is approximated by the NFAG and the TDE term is approximated by the planar Bouguer plate effect (BDE of Fig. 6) with chosen average constant density of 2200 kg/m^3 (cf. Eq. (6)). Since both the terms depend linearly on the vertical displacement field, they can be merged into

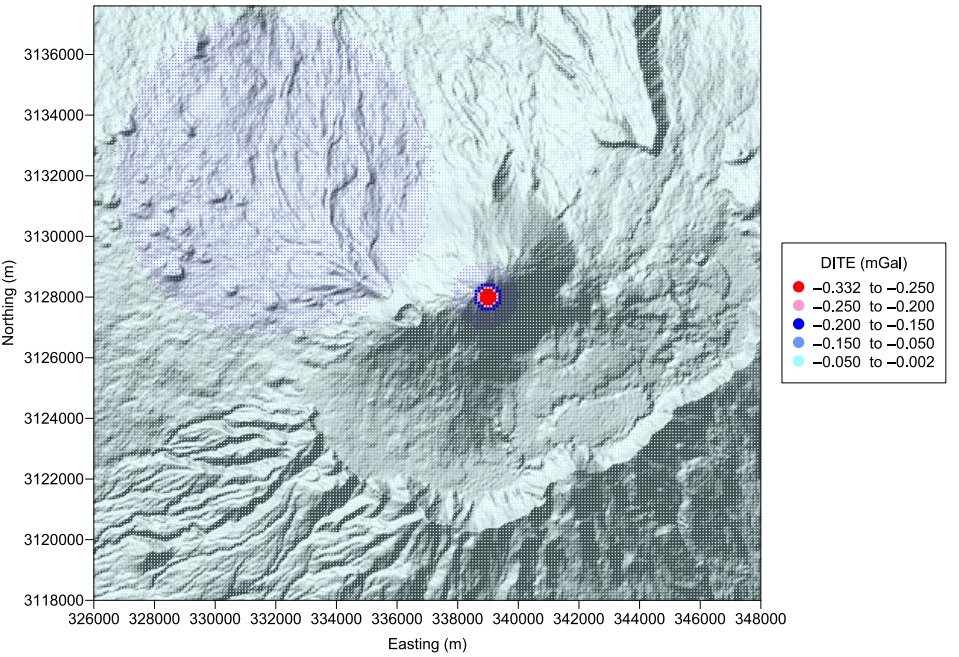

Fig. 8. The DITE (TN-DITE) for the displacement field of Fig. 4 (density 2200 kg/m^3). Max = −2, Min = −332, Mean = −30, SD = 29 (μGal).

one term based on the Bouguer-corrected NFAG (BCFAG):

$$\Delta g^{def}(P^*) \approx BCFAG(\rho_0) * \Delta h(P)\,, \tag{11}$$

computed for the displacement field of Fig. 4. In Fig. 12 we show the difference between the DITE (herein represented by the TN-DITE of Fig. 8) and the BCFAG approximation of DITE (Fig. 11) respective to the displacement field of Fig. 4.

5. Discussion and conclusions

We took a look here at the deformation induced topographic effect (DITE) on time-lapse gravity changes, by decomposing it into the Free Air Effect (FAE) and Topographic Deformation Effect (TDE), and assessing both com-

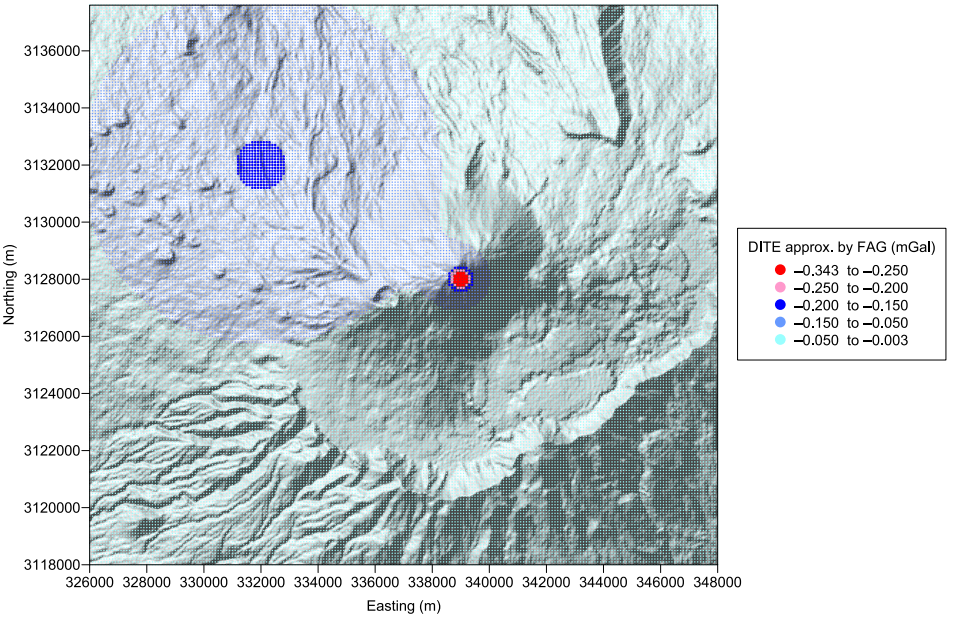

Fig. 9. The NFAG approximation of the DITE (cf. Eq. (10)), for the displacement field of Fig. 4. Max = −3, Min = −343, Mean = −39, SD = 37 (μGal).

ponents (effects) numerically by means of a case study situated in the Central Volcanic Complex (CVC) of Tenerife, and with the help of a simulated surface deformation field. We also assessed numerically the differences between the rigorous evaluation of the two effects and some approximations commonly used in practice.

Regarding the approximation of the true vertical gradient of gravity (VGG) in the FAE, we have assumed that the use of topographically corrected normal FAG (TNFAG) is a better option than the normal (theoretical) FAG (NFAG) in regions of rugged (significant) topography, such as the CVC of Tenerife, where the contribution of the topography to the VGG can be anticipated as higher than the contribution of the subsurface density anomalies (geological structure) to the VGG. The contribution of the topography to the VGG in an area like that of the studied CVC is at the level of 80 % of the NFAG. For this reason we propose that the NFAG approximation of the VGG is replaced by the TNFAG approximation of the VGG both in (a) the FAE when reducing the temporal gravity changes, and

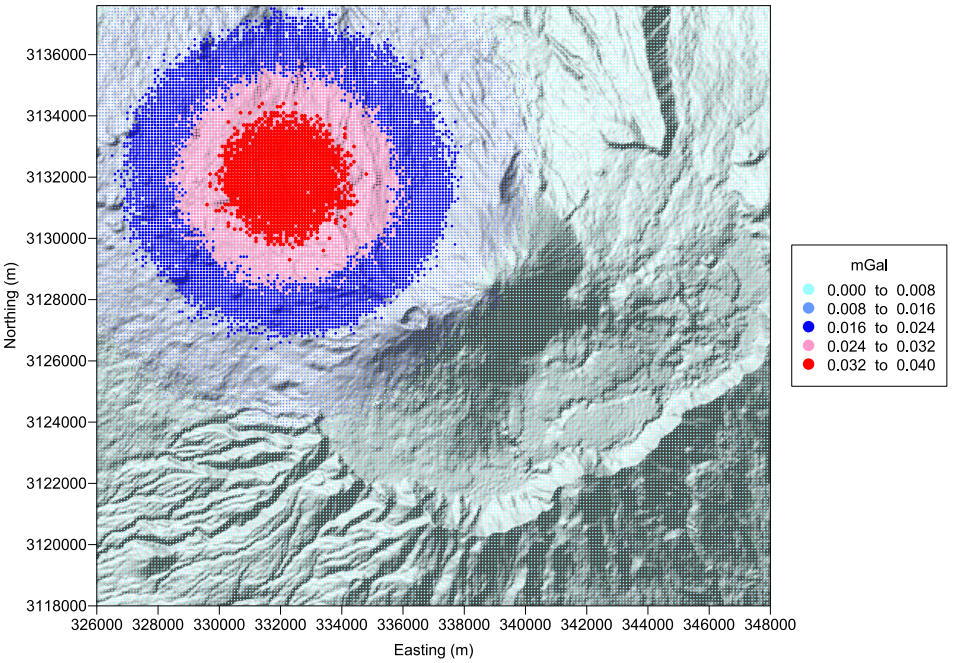

Fig. 10. The difference between the TN-DITE and the NFAG approximation of DITE, respective to the displacement field of Fig. 4. Max = 40, Min = 0, Mean = 9, SD = 9 (μGal).

(b) in reducing the observed gravity from the gravimeter sensor position to the ground, whenever the true (observed in situ) VGGs are not available at each gravity point (station/benchmark) of the survey. In a follow-up work we plan to observationally verify the relations between VGG, NFAG and TNFAG in our study area at the CVC of Tenerife and in other volcanic terrains/areas.

With respect to the second term of the DITE, the TDE, our synthetic numerical simulations made it apparent that the TDE must be computed via the Newton volumetric integration using a precise high resolution DEM. This effect varies sharply with the roughness of topography. An approximation by means of the planar or spherical Bouguer deformation effect (BDE) is simply not good enough.

The complete DITE, consisting of both the FAE and the TDE, should

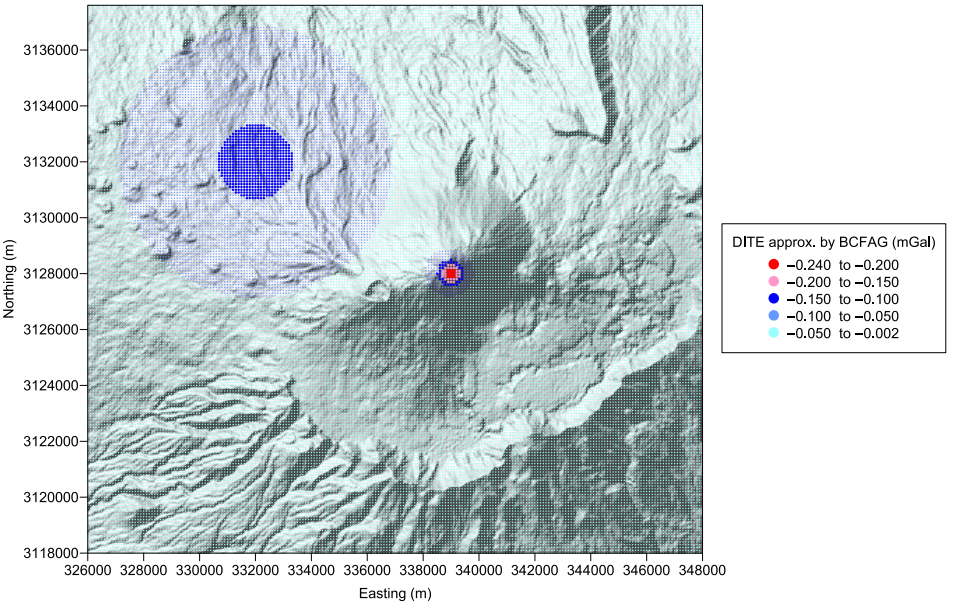

Fig. 11. The BCFAG approximation of DITE, respective to the displacement field of Fig. 4. Max = −2, Min = −240, Mean = −27, SD = 26 (μGal).

consequently be computed using the observed VGGs in the FAE term and the numerical Newtonian volumetric integration in the evaluation of the TDE. By synthetic numerical simulations we have compared the DITE to two approximations of DITE that would be typically used in practice when lacking the observed VGGs. Note that due to the lack of observed VGGs in our study region, FAE in the DITE is computed using the TNFAG approximation of the VGG – hence we have to speak about the TN-DITE representation of the true DITE in our comparisons. These comparisons based on the rigorously evaluated DITE based on observed VGGs in the FAE term are again left as a subject for our follow up work. Representing the rigorous DITE by the TN-DITE approximation, we have compared the DITE (TN-DITE) to (a) the NFAG approximation of DITE (cf. eqn. (10)) and (b) the BCFAG approximation of DITE (cf. eqn. (11)). We notice that the short-wavelength variability of the TDE (cf. Fig. 5) disappeared from the TN-DITE (cf. Fig. 8). It cancelled out with the short-wavelength variability of the topographic correction to the NFAG (ΔFAG^T). We shall

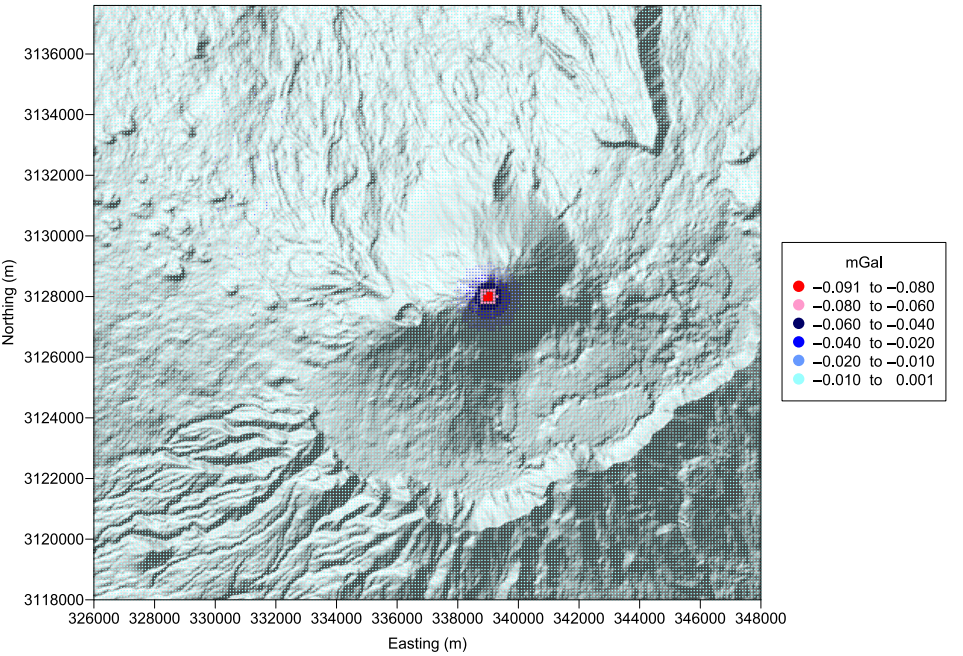

Fig. 12. The difference between the TN-DITE and the BCFAG approximation of DITE, respective to the displacement field of Fig. 4. Max = 1, Min = −91, Mean = −3, SD = 3 (μGal).

elaborate more on this finding in the follow-up work.

Figs. 10 and 12 indicate that the NFAG approximation of DITE works better for narrow sharp displacement fields (generated by shallow point sources), while the BCFAG approximation works better for displacement fields of larger horizontal extents of several kilometers (generated by deeper point sources). In other words, the situation with very local (sharp/narrow) deformation is closer to "normal free air" situation, while the larger areal deformation is better approximated using the Bouguer plate effect in addition to the normal free air ("Bouguer situation").

Acknowledgments. This work was supported by the Slovak Research and Development Agency (APVV) under projects No. APVV-0724-11 and APVV-0194-10 as well as by the VEGA grant agency under projects No. 2/0042/15, 1/0141/15, and 1/0642/13.

References

Battaglia M., Gottsmann J., Carbone D., Fernández J., 2008: 4D volcano gravimetry. Geophysics, **73**, 6, WA3–WA18, doi: 10.1190/1.2977792.

Battaglia M., Hill D. P., 2009: Analytical modeling of gravity changes and crustal deformation at volcanoes: The Long Valley caldera, California, case study. Tectonophysics, **471**,(1–2), 45–57, doi: 10.1016/j.tecto.2008.09.040.

Battaglia M., Segall P., Roberts C. W., 2003: The mechanics of unrest at Long Valley caldera, California. 2. Constraining the nature of the source using geodetic and micro-gravity data. *J. Volcanol. Geotherm. Res.*, **127**, 219–245.

Becker J. J., Sandwell D. T., Smith W. H. F., Braud J., Binder B., Depner J., Fabre D., Factor J., Ingalls S., Kim S-H., Ladner R., Marks K., Nelson S., Pharaoh A., Trimmer R., Von Rosenberg J., Wallace G., Weatherall P., 2009: Global Bathymetry and Elevation Data at 30 Arc Seconds Resolution: SRTM30_PLUS. Marine Geodesy, **32**, 4, 355–371.

Berrino G., 1994: Gravity changes induced by height-mass variations at the Campi Flegrei caldera. J. Volcanol. Geotherm. Res., **61**, 293–309.

Berrino G., Corrado G., Luongo G., Toro B., 1984: Ground deformation and gravity changes accompanying the 1982 Pozzuoli uplift. Bull. Volcanol., **47**, 187–200.

Berrino G., Rymer H., Brown G. C., Corrado G., 1992: Gravity-height correlations for unrest at calderas. J. Volcanol. Geotherm. Res., **53**, 11–26.

Boy J. P., Gegout P., Hinderer J., 2002: Reduction of surface gravity data from global atmospheric pressure loading. Geophys. J. Int., **149**, 534–545.

Currenti G., Del Negro C., Ganci G., 2007: Modeling of ground deformation and gravity fields using finite element method: an application to Etna volcano. Geophys. J. Int., **169**, 775–786.

Currenti G., Del Negro C., Ganci G., 2008: Finite element modeling of ground deformation and gravity field at Mt. Etna. Annals of Geophysics, **51**, 1, doi: 10.4401/ag-3037.

Dehant V., 1987: Tidal parameters for an inelastic Earth. Phys. Earth Planet. Int., **49**, 97–116.

Eggers A., 1987: Residual gravity changes and eruption magnitudes. J. Volc. Geotherm. Res., **33**, 201–216.

Gottsmann J., Berrino G., Rymer H., Williams-Jones G., 2003: Hazard assessment during caldera unrest at the Campi Flegrei, Italy: a contribution from gravity–height gradients. Earth Planet. Sci. Lett., **211**, 295–309.

Gottsmann J., Wooller L., Martí J., Fernández J., Camacho A. G., Gonzalez P. J., Garcia A., Rymer H., 2006: New evidence for the reawakenin of Teide volcano. Geophys. Res. Lett., **33**, L20311, doi: 10.1029/2006GL027523.

Gottsmann J., Camacho A. G., Martí J., Wooller L., Fernández J., García A., Rymer H., 2008: Shallow structure beneath the Central Volcanic Complex of Tenerife from new gravity data: Implications for its evolution and recent reactivation. Phys. Earth Planet. Int., **168**, 212–230.

Hagiwara Y., 1977: Gravity changes associated with seismic activities. In: C. Kisslinger and Z. Suzuki (editors), Earthquake Precursors. Adv. Earth Planet. Sci., **2**, 137–146.

Jarvis A., Reuter H. I., Nelson A., Guevara E., 2008: Hole-filled SRTM for the globe Version 4, available from the CGIAR-CSI SRTM 90m Database: <http://srtm.csi.cgiar.org>.

Jousset P., Okada H., 1999: Post-eruptive volcanic dome evolution as revealed by deformation and microgravity observations at Usu volcano (Hokkaido, Japan). J. Volcanol. and Geothermal Res., **89**, 255–273.

Jousset P., Dwip S., Beauducel F., Duquesnoy T., Diament M., 2000: Temporal gravity at Merapi during the 1993–1995 crisis: an insight into the dynamical behaviour of volcanoes. J. Volcanol. and Geothermal Res., **100**, 289–320.

Krause P., Naujoks M., Fink M., Kroner C., 2009: The impact of soil moisture changes on gravity residuals obtained with a superconducting gravimeter. J. Hydrol., **373**, 151–163, doi: 10.1016/j.jhydrol.2009.04.019.

Lampitelli C., Francis O., 2010: Hydrological effects on gravity and correlations between gravitational variations and level of the Alzette River at the station of Walferdange, Luxembourg. J. Geodynamics, **49**, 31–38, doi: 10.1016/j.jog.2009.08.003.

Leirião S., He X., Christiansen L., Andersen O. B., Bauer-Gottwein P., 2009: Calculation of the temporal gravity variation from spatially variable water storage change in soils and aquifers. J. Hydrol., **365**, 302–309, doi: 10.1016/j.jhydrol.2008.11.040.

Marušiak I., Zahorec P., Papčo J., Pašteka R., Mikuška R., 2013: Toposk, program for terrain corrections calculation, program guide. Manuscript, G-trend Ltd. (in Slovak).

Merriam J. B., 1992: Atmospheric pressure and gravity. Geophys. J. Int., **109**, 488–500.

Mogi K., 1958: Relations between the eruptions of various volcanoes and the deformations of the ground surfaces around them. Bull. Earthquake Res., Inst. Univ. Tokyo, **36**, 99–134.

Prutkin I., Vajda P., Gottsmann J., 2014: The gravimetric picture of magmatic and hydrothermal sources driving hybrid unrest on Tenerife in 2004/5. J. Volcanol. Geothermal Res., **282**, 9–18, doi: 10.1016/j.jvolgeores.2014.06.003.

Rymer H., 1994: Microgravity change as a precursor to volcanic activity. J. Volcanol. Geotherm. Res., **61**, 311–328.

Schiavone D., Capolongo D., Loddo M., 2009: Near-station topographic masses correction for high-accuracy gravimetric prospecting. Geophys. Prospecting, **57**, 739–752, doi: 10.1111/j.1365-2478.2009.00799.x.

Trasatti E., Bonafede M., 2008: Gravity changes due to overpressure sources in 3D heterogeneous media: application to Campi Flegrei caldera, Italy. Annals of Geophysics, **51**, 1, 119–133.

Umberto R., Berrino G., Corrado G., Hinderer J., 2008: Strategies in the processing and analysis of continuous gravity record in active volcanic areas: the case of Mt. Vesuvius. Annals of Geophysics, **51**, 1, 67–85.

Wahr J. M., 1981: Body tides on an elliptical, rotating, elastic and oceanless Earth. Geophys. J. R. Astr. Soc., **64**, 677–703.

Wenzel H. G., 1996: The NanoGal Software: Earth Tide Data Processing Package ETERNA 3.30. Bullettin d'Informations Mare'es Terrestres, Bruxelles, 9425–9438.

Williams-Jones G., Rymer H., 2002: Detecting volcanic eruption precursors: a new method using gravity and deformation measurements. J. Volcanol. Geothermal Res., **113**, 379–389.

Zahorec P., Papčo J., Mikolaj M., Pašteka R., Szalaiová V., 2014: Role of near topography and building effects in vertical gravity gradients approximation. First Break, **32**, 1, 65–71.